probe individual deep levels. As shown in Fig. 3A, three bright adatoms are visible. By performing spatial mapping of $I(Z)$ curves, we observe that the current intensity does not vary in the same manner for these three dangling bonds, as seen in the sequence of Fig. 3, D to H, corresponding to current intensity maps obtained at different tip-surface distances. For the dangling bonds labeled DB1 and DB2, their contrast begins to saturate after the tip has moved toward the surface by 3.05 Å (Fig. 3F) and 3.86 Å (Fig. 3G), respectively, whereas a halo, a sign of saturation, is seen at a higher tip displacement for dangling bond DB3 (Fig. 3H).

The saturation of the current intensity for the three dangling bonds is obtained from the plot of the $I(Z)$ curves in Fig. 3C. We find that the current intensity at saturation is four times higher on DB1 than on DB3. Although the spatial mapping of the $I(Z)$ curves cannot be recorded at the energy E_0 (*19*), similar variations are found when single $I(Z)$ spectra are measured on different dangling bonds at the energy E_0, as illustrated in fig. S1 (*20*). Thus, such a result indicates that the capture rate depends on the environment of the dangling bond.

To understand such variations of the capture rate, we acquired the image in Fig. 3B simultaneously with that in Fig. 3A. In this filled-state image, the three dangling bonds appear bright, but they are each surrounded by a dark region, with different spatial extents and depths. These regions are the signature of the Coulomb interaction between the charged dangling bonds and the free holes. The strength of this interaction is intimately related to the distribution of subsurface charged acceptors. As shown in (*8*), the acceptors appear as bright protrusions superimposed to the atomic corrugation of the Si adatoms in the filled-state STM image (Fig. 3B). Notably, two acceptors are found to be quite close from DB3, whereas no acceptor is visible around DB1. Such a distribution is quite consistent with the variation of the saturated current measured between the three dangling bonds and demonstrates that the potential fluctuations caused by the random distribution of B dopant atoms dramatically change the capture rate of a dangling bond.

By measuring similar $I(Z)$ curves for more than 90 dangling bonds, we found a distribution of the current intensities at saturation that is centered at 16 nA with a SD of 9 nA (Fig. 4). To explain this deviation, we analyzed the $I(Z)$ curves that were measured away from the bright Si adatoms. From the exponential tunneling behavior of these $I(Z)$ curves (see curves labeled BS and B_{Acc} in Fig. 3C), the spatial variations of the apparent barrier height are extracted (*21*) and yield a potential fluctuation range of 25 meV. Such fluctuations are expected to affect both the capture coefficient and the hole concentration. At 77 K, the capture cross section has a thermally activated behavior (*22*), and we estimate that the potential fluctuations induce a variation of the capture cross section by a factor of 1.4 (at most). Furthermore, the heavy doping of the Si sample yields a narrowing of the band gap of 130 meV. The potential fluctuations lead to a modification of the band gap narrowing, causing substantial variations of the hole concentration, which we estimate to range between 0.6×10^{20} and 1.7×10^{20} hole·cm^{-3} (*23*, *24*). Such variations of the capture cross section and hole concentration agree well with the measured distribution of the current intensities at saturation.

Although the capture rate is measured for a nonradiative recombination process involving the emission of vibrations, this new method is expected to be valid for the direct measurements of a wide range of carrier dynamic processes between a bound state and a continuum of states. It should be suitable to explore the capture and relaxation of charge carriers by the bound states of quantum dots or by point-defect states in nanostructures, such as nanowires, nanotubes, and single atomic sheets.

References and Notes

1. K. H. Schmidt, G. Medeiros-Ribeiro, M. Oestreich, P. M. Petroff, G. H. Dohler, *Phys. Rev. B* **54**, 11346 (1996).
2. C. Delerue, G. Allan, M. Lannoo, *Phys. Rev. B* **48**, 11024 (1993).
3. S. Coe, W. K. Woo, M. Bawendi, V. Bulovic, *Nature* **420**, 800 (2002).
4. S. M. Sze, *Physics of Semiconductor Devices* (Wiley, New York, ed. 2, 1981).
5. J. Bourgoin, M. Lannoo, *Point Defects in Semiconductors, Volume II: Experimental Aspects* (Springer-Verlag, Berlin, 1983).
6. H. G. Grimmeiss, C. Ovren, *J. Phys. E Sci. Instrum.* **14**, 1032 (1981).
7. I.-W. Lyo, E. Kaxiras, Ph. Avouris, *Phys. Rev. Lett.* **63**, 1261 (1989).
8. M. Berthe *et al.*, *Phys. Rev. Lett.* **97**, 206801 (2006).
9. I.-W. Lyo, Ph. Avouris, *Science* **245**, 1369 (1989).
10. J. Repp, G. Meyer, S. Paavilainen, F. E. Olsson, M. Persson, *Phys. Rev. Lett.* **95**, 225503 (2005).
11. X. de la Broise, C. Delerue, M. Lannoo, B. Grandidier, D. Stiévenard, *Phys. Rev. B* **61**, 2138 (2000).
12. I.-W. Lyo, Ph. Avouris, *Science* **253**, 173 (1991).
13. L. Limot, J. Kröger, R. Berndt, A. Garcia-Lekue, W. A. Hofer, *Phys. Rev. Lett.* **94**, 126102 (2005).
14. N. Néel *et al.*, *Phys. Rev. Lett.* **98**, 065502 (2007).
15. G. Mahieu *et al.*, *Phys. Rev. Lett.* **94**, 026407 (2005).
16. D. Goguenheim, M. Lannoo, *Phys. Rev. B* **44**, 1724 (1991).
17. C. H. Henry, D. V. Lang, *Phys. Rev. B* **15**, 989 (1977).
18. N. M. Johnson, D. J. Bartelink, J. P. McVittie, *J. Vac. Sci. Technol.* **16**, 1407 (1979).
19. Because there is no state in the band gap region when the tip is above the passivated adatoms, closing the feedback loop between two $I(Z)$ spectra leads to a tip crash for sample voltages below +1 V.
20. Additional results obtained at a temperature of 5 K are available as supporting material on *Science* Online.
21. The apparent barrier height is given by $\Phi \approx 0.95\left(\frac{d \ln I}{d \ln Z}\right)^2$.
22. D. Goguenheim, M. Lannoo, *J. Appl. Phys.* **68**, 1059 (1990).
23. J. Wagner, *Phys. Rev. B* **29**, 2002 (1984).
24. J. Wagner, J. A. del Alamo, *J. Appl. Phys.* **63**, 425 (1988).

25. R.S. acknowledges the financial support of the Institut de Recherche sur les Composants logiciels et matériels pour l'Information et la Communication Avancée.

Supporting Online Material

www.sciencemag.org/cgi/content/full/1151186/DC1
Figs. S1 and S2

1 October 2007; accepted 3 December 2007
Published online 13 December 2007;
10.1126/science.1151186
Include this information when citing this paper.

Spin Conservation Accounts for Aluminum Cluster Anion Reactivity Pattern with O_2

R. Burgert,[1] H. Schnöckel,[1]* A. Grubisic,[2] X. Li,[2] S. T. Stokes,[2] K. H. Bowen,[2] G. F. Ganteför,[3] B. Kiran,[4] P. Jena[5]

The reactivity pattern of small (~10 to 20 atoms) anionic aluminum clusters with oxygen has posed a long-standing puzzle. Those clusters with an odd number of atoms tend to react much more slowly than their even-numbered counterparts. We used Fourier transform ion cyclotron resonance mass spectrometry to show that spin conservation straightforwardly accounts for this trend. The reaction rate of odd-numbered clusters increased appreciably when singlet oxygen was used in place of ground-state (triplet) oxygen. Conversely, monohydride clusters Al_nH^-, in which addition of the hydrogen atom shifts the spin state by converting formerly open-shell structures to closed-shell ones (and vice versa), exhibited an opposing trend: The odd-*n* hydride clusters reacted more rapidly with triplet oxygen. These findings are supported by theoretical simulations and highlight the general importance of spin selection rules in mediating cluster reactivity.

Metal-atom clusters occupy a broad middle ground between small molecules and extended solids. Early mass spectrometric studies revealed certain atomic compositions that exhibited unusual stability and were therefore termed "magic." A framework analogous to the atomic shell-filling model has been successful in rationalizing many of these observations on the basis of electronic structure considerations; i.e., the valence electrons are governed by an average potential created by the residual positive charges. The result is a jellium-

like shell structure with "magic" electron numbers 2, 8, 20, 40, 70, etc. (*1*, *2*). Though these "magic" numbers were first recognized for metal clusters of sodium (*3*) and other metals containing s-valence electrons (e.g., Cu, Ag, Au), they have also been applied to Al clusters because there is an overlap of 3s and 3p orbitals for clusters containing more than nine atoms (*4*, *5*). Although the unusual stability of, e.g., Al_{13}^- with its 40 electrons has been well explained (*6*), for Al clusters in general, certain reactivity patterns remain puzzling. One of these is the odd/even effect whereby Al_n^- clusters with an odd number of Al atoms react much more slowly with oxygen than do even-numbered clusters (*7*–*9*). According to previous studies, the reactivity of large Al clusters with oxygen should be determined by two factors, namely, the energy required to remove an Al atom and the electron affinity of the cluster (*10*). However, these factors alone may not be sufficient to describe the observed odd/even effect. The reduced reactivity of the Al_{odd} clusters with triplet oxygen ($^3O_2$) was mentioned frequently in the literature (*11*), but to our knowledge, the role of the spin has not been considered in this context (*7*–*9*). Spin conservation was estimated to be negligible because for multielectron systems like clusters, intersystem crossing processes were expected to take place quickly so that the intermediate products should always have the lowest possible spin multiplicities. Here, we demonstrate that this concept should be reconsidered. Spin conservation has an essential influence not only on reactions of small molecules—textbook examples are the fast reaction of NO radical with O_2 and the low reaction rate between SO_2 and O_2—but also on Al clusters. Similar conclusions have been reached in a recent study on the reactions of several $Al_4H_n^-$ species with O_2 (*12*). To investigate this issue in more detail, we studied reactions between Al_nH^- clusters and triplet O_2 as well as those of mass-selected Al_{13}^- clusters with singlet O_2 by Fourier transform ion cyclotron resonance mass spectrometry (FT-ICR MS) and by quantum chemical calculations.

Our apparatus and cluster ion source have been described elsewhere (*13*, *14*). The experiments were performed under ultrahigh-vacuum (UHV) conditions, so that only a few collisions with other molecules (approximately one collision per 10 s per cluster) could occur (*13*, *14*). The reaction time can be expanded and primary steps followed. In this way, snapshots of the reaction processes are taken, i.e., cluster degradation due to the formation of molecular aluminum monoxide. Al_2O is known to be a prominent gas-phase species produced in high-temperature reactions of aluminum and oxygen (*15*).

By 1989, Castleman (*16*) and Jarrold (*7*) and their colleagues had respectively demonstrated that anionic and cationic Al cluster ions showed the above-mentioned odd/even effect in the presence of O_2. Hettich (*9*) confirmed this behavior for Al_n^- cluster ions through FT-ICR MS experiments (fig. S1). Motivated by these results, we examined this odd/even effect by exposing mass-selected Al_{13}^- and Al_{14}^- clusters, two representatives of the Al_{odd}^- and Al_{even}^- series, respectively, to an O_2 atmosphere at 10^{-8} mbar. Al_{13}^- clusters proved relatively inert (just as Castleman had reported), and only small traces of Al_9^- clusters (as reaction products) were detected during our FT-ICR MS investigations (Eq. 1).

$$^1Al_{13}^- + {}^3O_2 \rightarrow {}^3[Al_{13}\cdot O_2]^- \quad -0.36\ \text{eV} \quad (1a)$$

$$^3[Al_{13}\cdot O_2]^- \rightleftarrows {}^1Al_{13}O_2^- \quad \text{spin transition} \quad (1b)$$

$$^1Al_{13}O_2^- \rightarrow {}^1Al_9^- + 2\ {}^1Al_2O \quad (1c)$$

$$Al_{13}^-(g) + {}^3O_2 \rightarrow Al_9^-(g) + 2\ Al_2O(g) \quad (\mathbf{1})$$

$$^2Al_{14}^- + {}^3O_2 \rightarrow {}^2[Al_{14}\cdot O_2]^- \quad -2.76\ \text{eV} \quad (2a)$$

$$^2[Al_{14}\cdot O_2]^- \rightleftarrows {}^2Al_{14}O_2^- \quad (2b)$$

$$^2Al_{14}O_2^- \rightarrow {}^2Al_{10}^- + 2\ Al_2O \quad (2c)$$

$$Al_{14}^-(g) + {}^3O_2 \rightarrow Al_{10}^-(g) + 2\ Al_2O(g) \quad (\mathbf{2})$$

In contrast, we found that mass-selected Al_{14}^- clusters reacted spontaneously to give Al_{10}^- [and two Al_2O (*15*, *17*, *18*) equivalents] under the same conditions (Eq. 2).

Although Al_{13}^- is a "double magic" cluster (40 electrons fulfill the shell model and the topology represents a centered icosahedron) (*19*), and thus of particular importance, analogous findings were also found for reactions of other odd- and even-numbered clusters with O_2. Generally, all Al_{odd}^- clusters react much more slowly with triplet oxygen than do Al_{even}^- clusters.

To understand the experimental observations, we drafted the following spin conservation hypothesis. With its 40 valence electrons (closed shell), the spin multiplicity of the ground state of the Al_{13}^- cluster is a singlet (^1A_g) and is labeled by $^1Al_{13}^-$ in the text below. Correspondingly, $^2Al_{14}^-$ has a doublet ground state ($^2A''$) due to its one unpaired electron [detailed information on quantum chemical calculations and spin states is available in the supporting online material (fig. S3 and table S1)]. Initially, these species form adducts with $^3O_2$ with the associated oxygen molecule bound to the surface of the cluster (denoted by $[Al_{13}\cdot O_2]^-$ and $[Al_{14}\cdot O_2]^-$ in Eqs. 1a and 2a, respectively). Due to spin conservation restrictions (*20*), $^3[Al_{13}\cdot O_2]^-$ is formed in a triplet state and $^2[Al_{14}\cdot O_2]^-$ in a doublet state. Subsequently, the oxygen molecule dissociates on the surface of the structurally rearranging cluster (Eqs. 1b and 2b, respectively), causing the cluster to heat up and leading to fragmentation of the cluster (Eqs. 1c and 2c). Because $^3[Al_{13}\cdot O_2]^-$ is in a triplet state, whereas its energetically accessible fragments, Al_9^- and Al_2O, are all singlets, there must be a spin transition—an inherently slow process. The direct formation of $^1[Al_{13}\cdot O_2]^-$ (singlet state) from $^1Al_{13}^-$ and $^3O_2$ is spin forbidden and therefore unlikely to proceed, because spin-orbit coupling in the case of light metals like alumi-

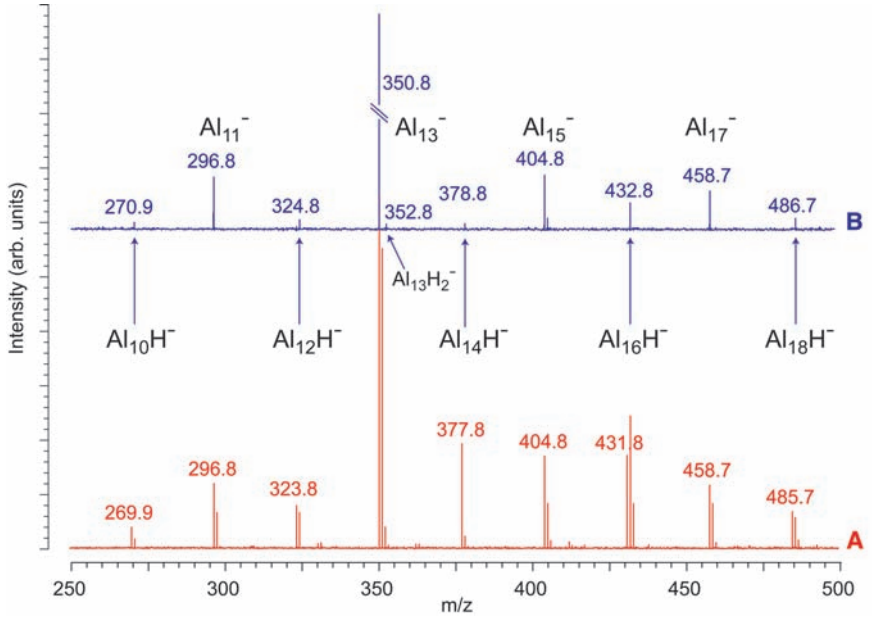

Fig. 1. Typical FT-ICR mass spectra after laser-desorption/ionization. (**A**) In the presence of H_2 as the collision gas during the cluster generation, $Al_nH_m^-$ clusters are formed. (**B**) After admitting $^3O_2$, all $Al_{odd}H^-$ react rapidly away. *m/z*, mass/charge ratio.

[1]Institute of Inorganic Chemistry, University of Karlsruhe (TH), 76128 Karlsruhe, Germany. [2]Departments of Chemistry and Materials Science, Johns Hopkins University, Baltimore, MD 21218, USA. [3]Department of Physics, University of Konstanz, 78457 Konstanz, Germany. [4]Department of Chemistry, McNeese State University, Lake Charles, LA 70605, USA. [5]Department of Physics, Virginia Commonwealth University, Richmond, VA 23284, USA.

*To whom correspondence should be addressed. E-mail: schnoeckel@chemie.uni-karlsruhe.de

num is small, preventing appreciable overlap between the potential energy surfaces (PESs) of different spin states (*20*). In contrast, in the case of Al_{14}^-, no such spin transition need occur because the initially formed $^2[Al_{14}{\cdot}O_2]^-$ can react directly via $^2Al_{14}O_2^-$ to form products $^2Al_{10}^-$ and Al_2O. We therefore hypothesized that for reactions of Al clusters with $^3O_2$, diminished rates are expected if the initially formed O_2 adduct is a triplet (due to spin conservation, e.g., $^3[Al_{13}{\cdot}O_2]^-$) and the final products are singlets (here, $^1Al_9^-$ and $^1Al_2O$).

To substantiate this idea experimentally, we manipulated the spin state of the aluminum-containing reactants by preparing aluminum hydride cluster anions, Al_nH^-, and exposed them to $^3O_2$; we changed the spin of O_2 by generating singlet oxygen ($^1O_2$), allowing it to react with Al_{13}^- and other odd-numbered Al_n^- clusters.

Upon addition of a hydrogen atom, the number of electrons in the cluster core changes by one, which also changes the spin state. We generated Al_nH^- clusters by reaction of Al_n^- clusters with hydrogen (Fig. 1A) (*21*). All $Al_{odd}H^-$ reacted rapidly with $^3O_2$, whereas $Al_{even}H^-$ proved inert. Thus, the reactivity pattern was notably inverted relative to Al_n^- behavior, e.g., $Al_{13}H^-$ reacted, even though Al_{13}^- (and $Al_{13}H_2^-$) had been nearly unreactive (Fig. 1B), whereas the initial $Al_{14}H^-$ signal remained unchanged, while Al_{14}^- reacted away (Eqs. 3 and 4). The observed universality of such behavior for these systems indicates that triplet oxygen reacts rapidly with all species in a doublet spin state (and possibly higher spin states), whereas it reacts much more slowly with species in a singlet state. The shell model considerations play a role as well by explaining the particularly unreactive character of certain clusters, most notably Al_{13}^-.

$$^2Al_{13}H^-(g) + {}^3O_2 \rightarrow {}^2[HAl_{13}{\cdot}O_2]^- \quad -1.93\ \text{eV} \quad (3a)$$

$$^2Al_{13}H^-(g) + {}^3O_2 \rightarrow {}^2Al_9H^-(g) + 2\ Al_2O(g) \quad (\mathbf{3})$$

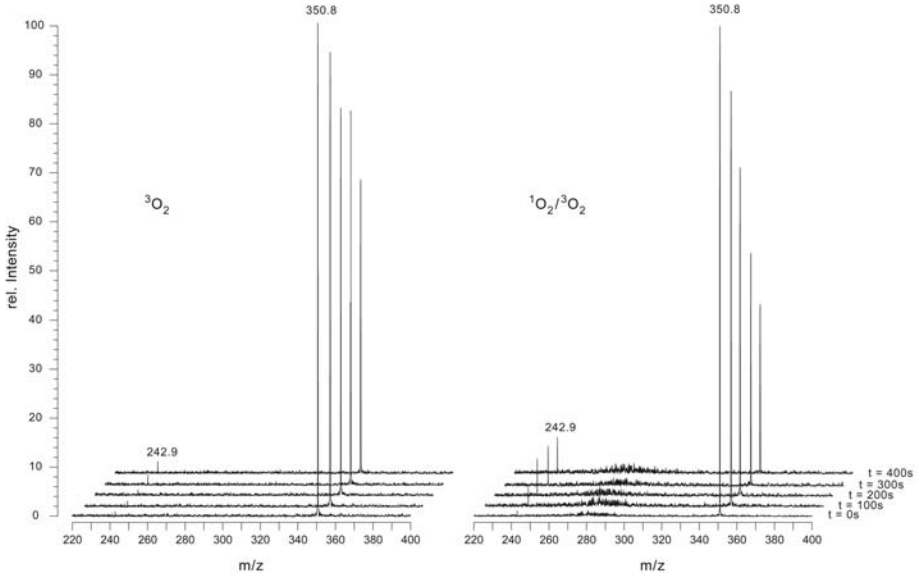

Fig. 2. Reactions of mass-selected Al_{13}^- clusters with $^3O_2$ (**left**) and with a $^1O_2/^3O_2$ mixture (**right**). The FT-ICR mass spectra show Al_9^- as the only major reaction product at *m/z* = 242.9 after up to 400 s of exposure to $^3O_2$ and $^1O_2/^3O_2$.

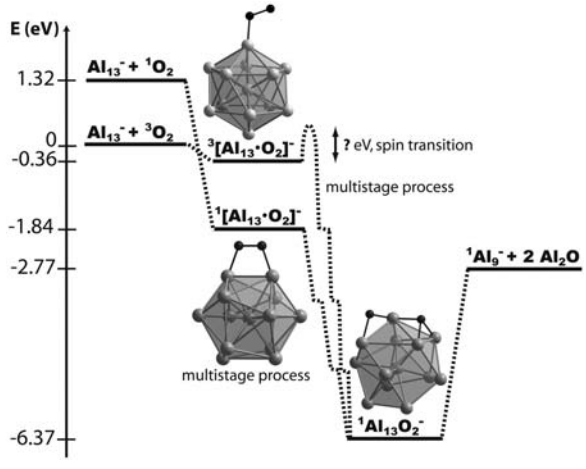

Fig. 3. Energy diagram (calculated) for the interaction of $^1O_2$ and $^3O_2$ on the Al_{13}^- cluster surface. The transition from $^3[Al_{13}{\cdot}O_2]^-$ to $^1Al_{13}O_2^-$ is estimated to be a multistage process in which O_2 is first bound side-on, then rearranges to end-on, after which the O-O bond is disrupted, new Al-O-bonds are formed (μ^3), and the spin state changes from triplet to singlet. In addition, the further degradation to Al_9^- and two Al_2O is displayed.

$$^1Al_{14}H^-(g) + {}^3O_2 \rightarrow {}^3[HAl_{14}{\cdot}O_2]^- \quad -1.43\ \text{eV} \quad (4a)$$

$$^1Al_{14}H^-(g) + {}^3O_2 \rightarrow {}^1Al_{10}H^-(g) + 2\ Al_2O(g) \quad (\mathbf{4})$$

$$^1Al_{13}^- + {}^1O_2 \rightarrow {}^1[Al_{13}{\cdot}O_2]^- \quad -3.16\ \text{eV} \quad (5a)$$

$$^1[Al_{13}{\cdot}O_2]^- \rightarrow {}^1Al_{13}O_2^- \quad -4.53\ \text{eV} \quad (5b)$$

$$^1Al_{13}O_2^- \rightarrow {}^1Al_9^- + 2\ Al_2O \quad 3.60\ \text{eV} \quad (5c)$$

$$^1Al_{13}^- + {}^1O_2 \rightarrow {}^1Al_9^- + 2\ Al_2O \quad -4.09\ \text{eV} \quad (\mathbf{5})$$

In the reaction of Al_{13}^- with $^1O_2$, $^1[Al_{13}{\cdot}O_2]^-$ is expected to form in its singlet state (Eq. 5a). In the course of further reaction through $^1Al_{13}O_2^-$ (in which O_2 is dissociated) to the products $^1Al_9^-$ and 2 Al_2O, all reaction steps are spin allowed (Eqs. 5b and 5c). In contrast to reactions with $^3O_2$, no spin transition is needed in the case of $^1O_2$, and therefore the reaction can proceed unimpeded.

Although $^1O_2$ is extremely short-lived in dense gases at pressures around 1 atm, the average lifetime of $^1O_2$ ($^1\Delta_g$) can be extended up to 3×10^3 s under collision-free conditions (pressure of ~10^{-8} mbar) (*22*), and experiments can be performed on this time scale. To generate $^1O_2$, we exposed $^3O_2$ to a static electrical discharge (Tesla coil) (*23*), yielding a $^1O_2/^3O_2$ mixture. Only $^1O_2$ molecules reacted at an appreciable rate with Al_{13}^-, and Al_9^- would be expected as the only product. As shown in Fig. 2, Al_{13}^- was degraded to Al_9^- in a $^1O_2$-containing atmosphere. The large excess of $^3O_2$ did not affect the experiment to an appreciable extent because the reaction of Al_{13}^- with $^3O_2$ is much slower [Fig. 2 (left)].

Tesla coil discharges can also induce formation of O atoms. If O atoms were to survive without reacting with the apparatus walls, they could potentially react with Al_{13}^- to form Al_{11}^- as indicated in Eq. 6. However, as shown in Fig. 2 (right), no Al_{11}^- formation was observed.

$$Al_{13}^-(g) + O \rightarrow Al_{11}^-(g) + Al_2O(g) \quad (\mathbf{6})$$

$$^1Al_{13}^- + {}^1O_3 \rightarrow {}^1Al_{11}^- + Al_2O + {}^1O_2 \quad (\mathbf{7})$$

$$^1Al_{11}^- + {}^1O_3 \rightarrow {}^1Al_9^- + Al_2O + {}^1O_2 \quad (\mathbf{8})$$

In addition, ozone (O_3) could be formed in the discharge as well (*23*). To characterize the reactivity of O_3, we exposed Al_{13}^- clusters to a pure O_3 atmosphere (*23*). This experiment showed that Al_{13}^- decomposed into Al_{11}^- and Al_9^-, as well as into Al_2O as coproduct (fig. S2 and Eqs. 7 and 8). Ozone has a singlet electronic ground state, and therefore all reaction steps are spin-allowed. As shown in Fig. 2 (right), Al_{11}^- is absent, indicating that O_3 was also not a major factor in the reaction of Al_{13}^- with the $^1O_2/^3O_2$ mixture. (*24*)

To support our experimental findings, we performed quantum chemical calculations at the second-order Møller-Plesset (MP2) level of theory with a triple-zeta polarization (TZVP) basis set using the Gaussian03 code (*25*). Coupled cluster with single, double and perturbative

triple excitations [CCSD(T)] single-point calculations were performed with the same basis set on MP2-optimized geometries. Unless otherwise noted, all energetic results reported here correspond to those obtained at the CCSD(T) level (*26*).

In modeling the odd/even effect, we assumed that the total reaction, wherein an Al_n^- cluster is reduced to two smaller fragments by oxygen, is a multistage process. In the initial step, O_2 interacts with the cluster to form an adduct, which further dissociates into the products Al_{n-4}^- and two Al_2O. The reactivity of a given cluster is determined by the nature of the initial interaction of O_2 with the cluster to form the adduct. Theoretical investigations on similar reactions between $^1O_2$ and unsaturated hydrocarbons (2 + 2 and 2 + 4 cycloadditions, "ene"-reactions) have revealed a puzzling array of reactive outcomes (*27*, *28*). Our calculations reveal that the initial interaction of O_2 with the cluster leads to an association complex, in which the O-O bond is slightly elongated, but remains intact (*29*). Subsequently, there is a strong bond formation between Al atoms and O_2, which is the rate-determining step. By comparison, the reaction of $^3O_2$ with C=C systems proceeds similarly, first through formation of a C-C-O-O adduct and then dissociation to products (*28*). Next, we calculated the reaction energies for each cluster. The spin-allowed interaction of $^1O_2$ with Al_{13}^- leading to formation of $^1[Al_{13}{\cdot}O_2]^-$ is calculated to be highly exothermic by −3.16 eV (Eq. 5a). Reactions of $^1O_2$ with carbon-carbon bonds are known to be concerted. Therefore, we assume that both O-Al bonds are formed simultaneously (Fig. 3). In subsequent reaction steps, both O atoms separate to give $^1Al_{13}O_2^-$ (Eq. 5b). This multistage process in which O_2 dissociates and covalent Al-O bonds are formed is also calculated to be highly exothermic (−4.53 eV). As experimentally observed, Al_9^- and 2 Al_2O molecules are formed as final products of this reaction cascade. The degradation of $^1Al_{13}O_2^-$ to these products is calculated to be endothermic by 3.60 eV (Eq. 5c). Thus, the net reaction is exothermic by −4.09 eV.

Concerning the association reaction of Al_{13}^- with $^3O_2$, we found that the initial interaction is only slightly exothermic by −0.36 eV (−35 kJ mol^{-1}) (Eq. 1a). In contrast to reactions of $^1O_2$, the $^3O_2$ diradical reacts through a consecutive pathway with only one O-Al bond being formed in the first step (Fig. 3). We calculated the formation of $^2Al_{14}O_2^-$ to be exothermic by −2.76 eV (−267 kJ mol^{-1}) (Eq. 2a).

For reactions of aluminum hydride clusters with $^3O_2$, we observed a similar trend, where the formation of $^3[HAl_{14}{\cdot}O_2]^-$ (triplet state) is less exothermic than the formation of $^2[HAl_{13}{\cdot}O_2]^-$ (doublet state) (Eqs. 3a and 4a).

The calculations indicate that on an aluminum hydride cluster surface, the initial interaction of oxygen is again less exothermic if the intermediate adduct is formed in a triplet state.

As demonstrated by the calculations (Fig. 3), the formation of $^1Al_{13}O_2^-$ is highly exothermic, but its total heat of formation (−7.69 eV) cannot be dissipated under UHV conditions; as a result, $^1Al_{13}O_2^-$ fragments by loss of two Al_2O molecules within a few nanoseconds (SOM Text, section 2). The cleavage of Al_2O is endothermic and will absorb much of that energy (3.60 eV). Though the above reactions are all spin-allowed, it is noteworthy that the highly exothermic formation of $^1[Al_{13}{\cdot}O_2]^-$ (singlet state) from Al_{13}^- and $^3O_2$ is not probable according to spin conservation rules (Eq. 1d).

The results of the calculations indicate that the formation of the initial oxygen adducts of all theoretically considered systems are exothermic and therefore spontaneous. Yet, observing that the exothermicity trend (Al_{14}^- > $Al_{13}H^-$ > $Al_{14}H^-$ > Al_{13}^-) closely parallels the trend of their reactivity toward oxygen (Al_{14}^- ~ $Al_{13}H^-$ > $Al_{14}H^-$ >> Al_{13}^-) led us to believe that although the spin-conservation factors must play a dominant role, to fully understand the kinetics of oxidation of these systems one has also to consider the energy factors. For example, systems forming a triplet initial adduct (e.g., Al_{13}^- and $Al_{14}H^-$) need to cross from their PES onto the PES of the singlet state (spin flip). As mentioned earlier, these transitions are inherently slow in light atom–containing species owing to their small spin-orbit coupling. In addition, crossing points between PESs of different spin states regularly occur at geometries different from that of the ground state, and therefore an energy barrier inherently accompanies these transitions. Consequently, a sufficient amount of energy is a necessary, yet not a sufficient condition, for spin flip reactions to proceed. For example, particularly stable systems such as the "double magic" Al_{13}^- do not release the required amount of energy upon adduct formation (−0.36 eV) to even reach the crossing point where the spin flip could occur. In contrast, the less-stable singlet systems such as $Al_{14}H^-$ and probably most other Al_{odd}^- and $Al_{even}H^-$ systems that release a considerable amount of energy upon adduct formation (e.g., −1.43 eV in the case of $Al_{14}H^-$) can likely reach the barrier energetically; however, these systems still suffer from the low probability of the transition between the two spin surfaces. This twofold control of kinetics could explain why among unreactive Al_{odd}^- and $Al_{even}H^-$ clusters, some clusters, most notably Al_{13}^-, prove particularly unreactive.

Thus, although the calculations could not fully illuminate the reactive pathway, they were nevertheless instructive and essentially supported our hypothesis: Reactions slow down if in accordance with spin conservation rules, the initial O_2 adduct is formed in a triplet state. This is true for pure Al clusters, as well as for Al cluster hydrides. When Al_{13}^- or $Al_{14}H^-$ react with $^3O_2$, the intermediate adducts are formed in a triplet state. Because the final products of these reactions are all in singlet states, there must be a spin transition in the course of the reaction cascades. In the case of $Al_{14}H^-$, the formation of $^3[HAl_{14}{\cdot}O_2]^-$ is exothermic by −1.43 eV. This step provides sufficient energy to eventually undergo a spin transition. Therefore, it is not surprising that reactions of $Al_{14}H^-$ and $^3O_2$ are slow in comparison with Al_{14}^-, but are much faster than reactions of Al_{13}^-, for which formation of $^3[Al_{13}{\cdot}O_2]^-$ is less exothermic (−0.36 eV).

In conclusion, we have shown that the reactivity of Al_n^- clusters with $^3O_2$ exhibits an odd/even trend that gets inverted upon addition of a single hydrogen atom. We furthermore demonstrated that Al_{13}^-, which reacts negligibly with $^3O_2$, reacts much more rapidly when exposed to even a small amount of $^1O_2$. These findings together represent direct experimental proof of the importance of spin in explaining the odd/even pattern observed for reactivities of Al clusters toward oxygen. It remains to be seen whether other systems can be experimentally shown to undergo similar selectivity. However, we speculate that as long as the reactant molecule exhibits a triplet state and the cluster series alternates in spin states, the spin restrictions may become crucial and cause clusters to exhibit the odd/even effect. In support of this idea, our recent study of similarly exothermic reactions of mass-selected Al_n^- clusters with Cl_2 showed only small differences in reactivities of neighboring Al clusters, agreeing with our expectations for a reactant in a singlet state ($^1Cl_2$) (*13*).

One implication of our study may have relevant consequences for catalysis. For example, deposited nanoparticles, clusters, or surface sites that possess specific spin states may exhibit highly selective catalytic behavior, arising from the difficulty of metal clusters containing light elements like aluminum to undergo a spin flip during the primary steps of a reaction (*20*). For clusters of heavier metal atoms with considerable spin-orbit coupling, this kind of selectivity may not be possible. Another important result is revealed when comparing the "double magic" Al_{13}^- super atom with the bulk metal (SOM Text, section 1). In both cases, there are marked topological (e.g., coordination number of the central atom is 12) and thermodynamic similarities (*13*, *14*) [e.g., the formation of solid Al_2O_3 from Al_{metal} and Al_{13}^- exhibits nearly the same reaction enthalpy $\Delta_R H^\circ$ (0 K): Eq. 9 (−3399 kJ mol^{-1}) and Eq. 10 (−3351 kJ mol^{-1})]. Within the error margin (theory and experiment), these enthalpy values equal the energy differences presented in Eqs. 1 to 5, 9, and 10. (Eqs. 9 and 10):

$$Al_{13}^-(g) + 3\ O_2 \rightarrow Al_9^-(g) + 2\ Al_2O_3(s) \quad -35.2\ eV \qquad (9)$$

$$4\ Al(bulk) + 3\ O_2 \rightarrow 2\ Al_2O_3(s) \quad -34.7\ eV \qquad (10)$$

Thus, Al_{13}^- may provide a suitable model for some aspects of the surface of bulk Al. If so, there may be an analogy between the slow reaction of

$^3O_2$ with bulk Al (*30*) and with the Al_{13}^- cluster. Because the interpretation of the low bulk reactivity remains unsettled, the results presented here may prove useful in unraveling the controversy surrounding the interpretation of solid-state aluminum reactivity. Furthermore, spin states play an important role in long-known oxidation processes (e.g., O_2/NO/NO_2; O_2/SO_2/SO_3), and also in the oxidation of carbon compounds: The first detailed experimental and theoretical data for $^1O_2$ reactions with 2 + 4 and 2 + 2 cycloadditions were presented only a decade ago (*28*). Thus, the present results may initiate further FT-ICR investigations of $^1O_2$ and $^3O_2$ reactions in many other chemical oxidation processes that affect our daily lives, e.g., in biology (respiration), engineering (corrosion), and energetics (combustion).

References and Notes

1. M. Brack, *Rev. Mod. Phys.* **65**, 677 (1993).
2. W. A. de Heer, *Rev. Mod. Phys.* **65**, 611 (1993).
3. T. P. Martin, *Phys. Rep.* **273**, 199 (1996).
4. R. Ahlrichs, S. D. Elliott, *Phys. Chem. Chem. Phys.* **1**, 13 (1999).
5. X. Li, H. Wu, X.-B. Wang, L.-S. Wang, *Phys. Rev. Lett.* **81**, 1909 (1998).
6. D. E. Bergeron, A. W. J. Castleman, T. Morisato, S. N. Khanna, *Science* **304**, 84 (2004).
7. M. F. Jarrold, J. E. Bower, *Chem. Phys. Lett.* **144**, 311 (1988).
8. R. E. Leuchtner, A. C. Harms, A. W. Castleman Jr., *J. Chem. Phys.* **94**, 1093 (1991).
9. R. L. Hettich, *J. Am. Chem. Soc.* **111**, 8582 (1989).
10. C. Ashman, S. N. Khanna, M. R. Pederson, *Chem. Phys. Lett.* **324**, 137 (2000).
11. We use the abbreviations Al_{even} and Al_{odd} to denote Al_n^- clusters with an even or odd number of Al atoms. The spin multiplicities of molecular entities are denoted by superscription, e.g., triplet oxygen by $^3O_2$.
12. A. C. Reber, S. N. Khanna, P. J. Roach, W. H. Woodward, A. W. Castleman Jr., *J. Am. Chem. Soc.* **129**, 16098 (2007).
13. R. Burgert, H. Schnöckel, M. Olzmann, K. H. Bowen Jr., *Angew. Chem. Int. Ed.* **45**, 1476 (2006).
14. R. Burgert, S. T. Stokes, K. H. Bowen, H. Schnöckel, *J. Am. Chem. Soc.* **128**, 7904 (2006).
15. M. W. Chase Jr., in *NIST-JANAF Thermochemical Tables, J. Phys. Chem. Ref. Data, Monograph 9*. (1998), pp. 1–1951.
16. R. E. Leuchtner, A. C. Harms, A. W. Castleman Jr., *J. Chem. Phys.* **91**, 2753 (1989).
17. G. H. Peslherbe, W. L. Hase, *J. Phys. Chem. A* **104**, 10556 (2000).
18. Although neutral species cannot be directly observed in our experiment, Al_2O, as the likely neutral by-product of the oxidation of Al clusters, was indirectly inferred from the following: (i) By performing the experiments under ultralow-pressure conditions, one can ensure that only few collisions of clusters with O_2 occur (~1 per second), thereby excluding the possibility of involvement of more than one O_2 molecule per reaction event. Consequently, observing that oxidation of Al_n^- clusters yields $Al_{(n-4)}^-$ implies concomitant formation of a neutral fragment, Al_4O_2, or several fragments stoichiometrically equivalent to Al_4O_2. (ii) According to the phase space theory, the validity of which was confirmed for Al clusters (*17*), the formation of Al_4O_2 (instead of two Al_2O) is unlikely, because the average lifetime of an $Al_{13}O_2^-$ or $Al_{14}O_2^-$ adduct with respect to this reaction channel is estimated to be some years (see calculations in SOM Text, section 2). (iii) The formation of Al atoms during degradation of the $Al_{13}O_2^-$ clusters toward Al_9^- can be excluded by thermodynamical reasons (SOM Text, section 3).
19. E. G. Mednikov, M. C. Jewell, L. F. Dahl, *J. Am. Chem. Soc.* **129**, 11619 (2007).
20. H. Schwarz, *Int. J. Mass Spectrom.* **237**, 75 (2004).
21. X. Li *et al.*, *Science* **315**, 356 (2007).
22. H. Okabe, in *Photochemistry of Small Molecules* (Wiley, New York, 1978), pp. 431–432.
23. R. Ahlrichs, C. Ehrhardt, M. Lakenbrink, S. Schunck, H. Schnöckel, *J. Am. Chem. Soc.* **108**, 3596 (1986).
24. Because there is a large excess of O_3 compared to the Al cluster anions, too few $^1O_2$ molecules are formed as coproducts to induce undesired reactions.
25. M. J. Frisch *et al.*, Gaussian 03, Revision C.02; Gaussian, Inc., Wallingford, CT (2004).
26. All the CCSD(T) calculations were done with NWChem 5.1 using the Computers at Molecular Science Computing Facility (MCSF) in Environmental Molecular Science Laboratory (EMSL), a national scientific user facility sponsored by the U.S. Department of Energy (DOE), Office of Biological and Environmental Research (OBER), and located at Pacific Northwest National Laboratory.
27. W. Adam, *Chem. Unserer Zeit* **15**, 190 (1981).
28. A. Greer, *Acc. Chem. Res.* **39**, 797 (2006).
29. There is a lack of reliable methods to calculate the height of this barrier. However, for similar reactions in organic chemistry, this barrier is indicated to be 0.8 eV (*27*).
30. J. Behler, B. Delley, S. Lorenz, K. Reuter, M. Scheffler, *Phys. Rev. Lett.* **94**, 036104/1 (2005).

31. H.S. acknowledges M. Olzmann for helpful discussions. H.S. and G.F.G. thank the Deutsche Forschungsgemeinschaft (DFG) and the DFG–Center for Functional Nanostructures (H.S.) for their support of this work. K.H.B. thanks the Air Force Office of Scientific Research for its support. P.J. thanks the U.S. DOE for its support.

Supporting Online Material

www.sciencemag.org/cgi/content/full/319/5862/438/DC1
SOM Text
Figs. S1 to S3
Table S1
References

1 August 2007; accepted 14 December 2007
10.1126/science.1148643

NMR Imaging of Catalytic Hydrogenation in Microreactors with the Use of para-Hydrogen

Louis-S. Bouchard,[1]* Scott R. Burt,[1] M. Sabieh Anwar,[2] Kirill V. Kovtunov,[3] Igor V. Koptyug,[3] Alexander Pines[1]*

Catalysis is vital to industrial chemistry, and the optimization of catalytic reactors attracts considerable resources. It has proven challenging to correlate the active regions in heterogeneous catalyst beds with morphology and to monitor multistep reactions within the bed. We demonstrate techniques, using magnetic resonance imaging and para-hydrogen (p-H_2) polarization, that allow direct visualization of gas-phase flow and the density of active catalyst in a packed-bed microreactor, as well as control over the dynamics of the polarized state in space and time to facilitate the study of subsequent reactions. These procedures are suitable for characterizing reactors and reactions in microfluidic devices where low sensitivity of conventional magnetic resonance would otherwise be the limiting factor.

Catalysis is a fundamental component to many industrial processes and, consequently, the optimization of catalytic reactions and reactors attracts considerable technological effort and financial commitments. An important aspect of this optimization is to correlate the spatial distribution of the reactive conversion inside the reactor with the morphology and packing of the catalyst. Here, we describe a spectroscopic method for this purpose based on magnetic resonance imaging (MRI) (*1*) that uses hyperpolarized spins derived from p-H_2 (*2*, *3*). Specifically, we achieve high-resolution, spatially resolved profiles of heterogeneous hydrogenation reactions taking place at a solid-gas interface inside a microreactor. We demonstrate strongly enhanced nuclear magnetic resonance (NMR) signal intensities in the gas phase as well as precise control over the spatiotemporal dynamics of the polarization. The enhanced sensitivity is particularly important for tracking gases and products in small volumes [e.g., in microfluidic devices (*4*, *5*) or the limited void space of a tightly packed catalyst bed]. Moreover, the controlled delivery of p-H_2–induced nuclear spin polarization acts as a spin label that can transport polarization to remote regions in the reactor. This work has implications for studying kinetics and mechanisms of multistep heterogeneously catalyzed reactions and fluid-flow transport, as well as mass and heat transfer. Such characterization should facilitate improved reactor and catalyst design.

Methods to optimize microreactors would be welcome in the context of microfluidic (lab-on-a-chip) technology. In recent years, the compelling advantages of microfluidic technology (*4*, *5*) in biopharmaceutical applications, chemical analysis (*6*), organic synthesis (*7*, *8*), and industrial catalysis have been recognized and demonstrated

[1]Materials Sciences Division, Lawrence Berkeley National Laboratory and Department of Chemistry, University of California, Berkeley, CA 94720, USA. [2]School of Science and Engineering, Lahore University of Management & Sciences, Opposite Sector U, D.H.A., Lahore 54792, Pakistan. [3]International Tomography Center, 3A Institutskaya Street, Novosibirsk 630090, Russia.

*To whom correspondence should be addressed. E-mail: louis.bouchard@gmail.com (L.-S.B.); pines@berkeley.edu (A.P.)